Femtosecond photoelectron spectroscopy of the I_2^- anion: Characterization of the $\tilde{A}'\,^2\Pi_{g,1/2}$ excited state

Martin T. Zanni, Victor S. Batista, B. Jefferys Greenblatt, William H. Miller, and Daniel M. Neumark
Department of Chemistry, University of California, Berkeley, California 94720 and Chemical Sciences Division, Lawrence Berkeley National Laboratory, Berkeley, California 94720

(Received 21 September 1998; accepted 9 November 1998)

A potential energy curve for the $\tilde{A}'\,^2\Pi_{g,1/2}$ state of I_2^- is constructed based on femtosecond photoelectron spectroscopy of the I_2^- $\tilde{A}'\,^2\Pi_{g,1/2} \leftarrow \tilde{X}\,^2\Sigma_u^+$ transition at 780 nm. The experiment is sensitive to the slope of the repulsive potential wall, the well depth, equilibrium bond length, and the long-range attractive portion of the upper state potential. The $\tilde{A}'\,^2\Pi_{g,1/2}$ potential is fit to a piecewise potential which is flexible in each of these regions. Simulations of the spectrum using a previously determined Morse potential for the $\tilde{X}\,^2\Sigma_u^+$ state of I_2^- [J. Chem. Phys. **107**, 7613 (1997)] yields a well depth (D_e) of 0.017 ± 0.010 eV for the $\tilde{A}'\,^2\Pi_{g,1/2}$ state with an equilibrium bond length (R_e) of 6.2 ± 0.6 Å. These values differ significantly from previous semiempirical results. © *1999 American Institute of Physics.* [S0021-9606(99)00207-X]

I. INTRODUCTION

Photodissociation of iodine in clusters,[1,2] liquids,[3–10] and matrices[11,12] has for many years been a model system for the study of caging, recombination, and vibrational relaxation. In I_2^-, the analogous negative ion system, the effect of much stronger solvent/solute interactions on these processes has been explored in size-selected clusters of $I_2^-(Ar)_n$,[13,14] $I_2^-(CO_2)_n$,[13,15–17] $I_2^-(OCS)_n$,[18] and in several polar solvents.[19–21] The vibrational relaxation of I_2^- photofragments created by the photodissociation of I_3^- has also been studied in liquids.[22–24] The interpretation and theoretical modeling of all of these experiments, however, relies at least in part on accurate ground and excited state potential energy curves for I_2^-. We have recently reported an accurate ground state potential for I_2^-,[25] but the available empirical excited state potentials are at best approximately correct.[26–28] In this study, we apply femtosecond photoelectron spectroscopy (FPES) to the photodissociation of I_2^-, and simulate our experimental results using an improved quantum mechanical simulation method. The experimental results are of considerably higher quality than those reported by us previously.[29] The new results in conjunction with the simulations enables us to generate the first quantitative potential for the $I_2^-(\tilde{A}'\,^2\Pi_{g,1/2})$ excited state.

The FPES experiment involves photoexcitation of I_2^- from its ground $\tilde{X}\,^2\Sigma_u^+$ state to the dissociative $\tilde{A}'\,^2\Pi_{g,1/2}$ state with a femtosecond pump pulse at 780 nm. The photoelectron spectrum of the dissociating molecule is measured at a series of delay times by photodetachment with a femtosecond probe pulse. The variation of the photoelectron spectrum with delay time monitors the dissociating anion from the initial Franck–Condon region of excitation out to the asymptotic product channel of $I^- + I$. Hence one can, in principle, probe the excited state potential over the entire reaction coordinate.

The anion and neutral states potentials relevant to our experiment are shown in Fig. 1. Most of the neutral I_2 states which correlate to $I(^2P_{3/2}) + I(^2P_{3/2})$ products are well characterized,[30–36] as is the ground state of the anion,[25] leaving the excited anion surface the most uncertain. There exist several previously reported empirical and *ab initio* potentials for the excited states of I_2^-. Chen and Wentworth have published semiempirical potentials based on a wide range of experimental data including electronic spectroscopy in crystals and gas phase dissociative attachment experiments.[26] Since their original publication in 1985, they have twice updated the potentials for these states using more recent experimental data.[27,28] The potentials remain largely uncertain, however, since they are composed of at most four experimental parameters.

Several *ab initio* studies have also been performed on I_2^-. These include valence bond methods by Tasker *et al.*,[37] self-consistent field (SCF) calculations by Bowmaker *et al.*,[38] and relativistic core potentials by Shaik and co-workers.[39] These studies are complicated, however, because of the large number of electrons and strong spin–orbit coupling in I_2^-. Spin-orbit effects were explicitly included in a multireference configuration interaction calculation of the I_2^- potentials by Maslen *et al.*[40] These potentials have been recently improved[41,42] by scaling the *ab initio* curves to reproduce the experimental equilibrium bond length and well depth for the $\tilde{X}\,^2\Sigma_u^+$ state,[25] while maintaining the *ab initio* energy spacings. The resulting potential for the $I_2^-(\tilde{A}'\,^2\Pi_{g,1/2})$ state has a shallow well at long internuclear distance, $D_e = 19.5$ meV and $R_e = 6.8$ Å. Simulations[43] on the scaled potentials yield reasonable agreement with our original FPES study of I_2^-,[29] particularly at early time delays.

We have previously reported on the I_2^- $\tilde{A}'\,^2\Pi_{g,1/2} \leftarrow \tilde{X}\,^2\Sigma_u^+$ photodissociation at 780 nm studied with FPES.[29] Since then, the experimental resolution has been improved

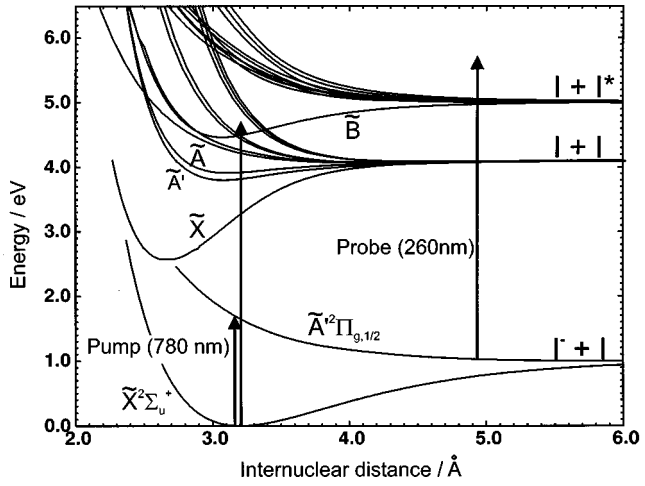

FIG. 1. Potential energy curves for the I_2 and I_2^- electronic states relevant to the discussion (Refs. 25, 30–36, 53). Only the $\tilde{X}\,{}^1\Sigma_g^+$, $\tilde{A}'\,{}^3\Pi_{2u}$, $\tilde{A}\,{}^3\Pi_{1u}$, and $\tilde{B}\,{}^3\Pi_{0^+u}$ states of I_2 are labeled. The 260 nm probe is shown detaching the ground and excited state potentials of I_2^-.

by more than a factor of 3. In addition, our ability to simulate the spectra has improved significantly for several reasons. First, we now have a more accurate potential[25] for the ground state of I_2^- than was available at the time of the original study. Secondly, the quantum mechanical simulation method originally used was extremely time-consuming, and the simulations performed included photodetachment transitions to only three of the 20 neutral I_2 electronic states that correlate to $I(^2P_{3/2})+I(^2P_{3/2})$ and $I(^2P_{3/2})+I^*(^2P_{1/2})$ products, namely, the $\tilde{A}'\,{}^3\Pi_{2u}$, $\tilde{A}\,{}^3\Pi_{1u}$, and $\tilde{B}'\,{}^3\Pi_{0^-u}$ states. The improved quantum mechanical simulation method described in our accompanying paper[44] is considerably more efficient, and the simulations reported here incorporate photodetachment to all 20 relevant states of I_2. Finally, we have developed an empirical functional form to reproduce our experimental resolution, and thus more faithfully convolute our simulations for comparison with experiment. These improvements in the experiment and analysis result in a definitive characterization of the $I_2^-(\tilde{A}'\,{}^2\Pi_{g,1/2})$ state.

II. EXPERIMENT

The FPES experiment consists of two major components; a negative ion photoelectron spectrometer and a high repetition rate femtosecond laser. Each has been described in detail elsewhere and will be discussed only briefly below.[17,25]

The photoelectron spectrometer has been optimized to be compatible with the high laser repetition rate (500 Hz in these experiments) and the low photoelectron signal expected for a two-photon pump-and-probe experiment. Argon carrier gas (10 psig) is passed over crystalline I_2 and supersonically expanded through a pulsed piezoelectric valve operating at a repetition rate of 500 Hz.[45] Anions are generated by a 1 keV electron beam which crosses the expansion just downstream of the nozzle, and are injected into a Wiley–McLaren time-of-flight mass spectrometer[46] by applying pulsed extraction and acceleration fields perpendicular to the molecular beam axis. After passing through several differentially pumped regions, the ions enter the detector chamber where they are dissociated with the pump laser pulse and detached with the probe laser pulse. The ions are monitored with a retractable, in-line microchannel plate detector. High electron collection efficiency is achieved with a ''magnetic bottle'' time-of-flight analyzer[47] whose energy resolution has been optimized using a pulsed decelerator[48,49] applied to the ions just prior to photodetachment. The instrument resolution is determined by photodetachment of I^- with 390 and 260 nm light. This produces three atomic peaks at 0.12, 0.77, and 1.71 eV whose widths increase with electron kinetic energy. Their widths are 20, 50, and 76 meV, respectively. These three peaks are used to convolute the simulated FPES spectra as described in Sec. IV B.

The pump and probe laser pulses are obtained from a Clark-MXR regeneratively amplified Ti:Sapphire laser system, which generates pulses at 780 nm (1.59 eV) with 1 mJ energy and 80 fs (sech^2) width. About 150 μJ of this is used as the pump pulse. The probe pulse is generated by frequency-tripling the remainder of the 780 nm fundamental, producing pulses at 260 nm (4.77 eV), with 20 μJ energy, and 130 fs width (the latter measured by difference frequency mixing with the fundamental light). The relative delay between the pump and probe pulses is adjusted with a computer controlled translation stage, and the beams are collinearly recombined prior to entering the vacuum chamber. The probe pulse has enough energy to detach the I^- products as well as ground state I_2^-, which produces a background spectrum. By passing the pump beam through a 250 Hz chopper (New Focus, 3501), shot-to-shot subtraction of the background photoelectron signal is performed. The background signal is also integrated and used to normalize different scans.

The vacuum chamber window affects the individual pulse widths and the relative delay between the pump and probe pulses. To characterize the pulses and determine the zero-of-time inside the chamber, two-color above-threshold detachment of I^- is used.[50] The probe pulse alone produces a photoelectron spectrum with two peaks at 0.77 and 1.71 eV. When the pump and probe pulses are temporally overlapped, additional peaks are observed that correspond to shifting the I^- peaks by 1.59 eV towards higher eKE; i.e. the photon energy of the pump pulse. From the intensity of this two-color signal as a function of pump–probe delay, we determine the zero-delay time and the cross-correlation of the pump and probe pulses inside the vacuum chamber. This yields a convoluted FWHM of 175 fs.

III. RESULTS

Figure 2 (solid) shows successive femtosecond photoelectron spectra, plotted as a function of electron kinetic energy, and taken at increasingly larger pump–probe delay times. Also included in Fig. 2 (dotted and dashed) are the simulated spectra, which will be discussed in Sec. IV. At the bottom of the figure, the experimental background spectrum arising from detachment of ground state I_2^- by the probe pulse is shown, and the peaks labeled A, B, and C in the

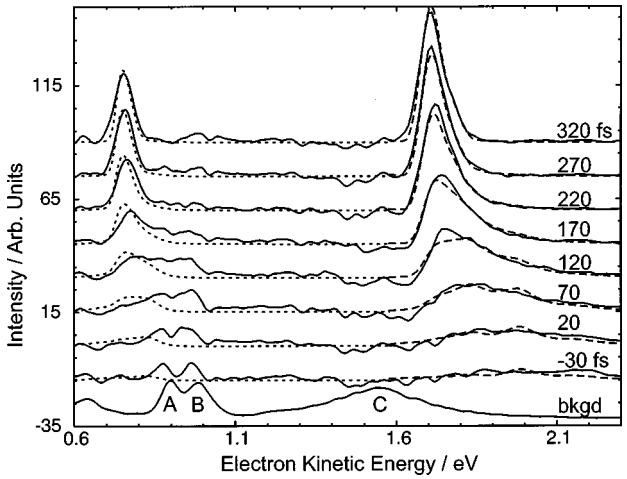

FIG. 2. Experimental femtosecond photoelectron spectrum taken at various pump–probe delay times (solid). The background spectrum from detachment of ground state I_2^- by the 260 nm probe pulse is also shown (bottom). The peaks labeled A, B, and C result from detachment to the $\tilde{A}\,^3\Pi_{1u}$, $\tilde{A}'\,^3\Pi_{2u}$, and $\tilde{X}\,^1\Sigma_g^+$ states of I_2, respectively. Simulated spectra used to characterize the $I_2^-(\tilde{A}'\,^2\Pi_{g,1/2})$ state (dashed), and simulations used to evaluate the *ab initio* potentials (dotted) are also shown.

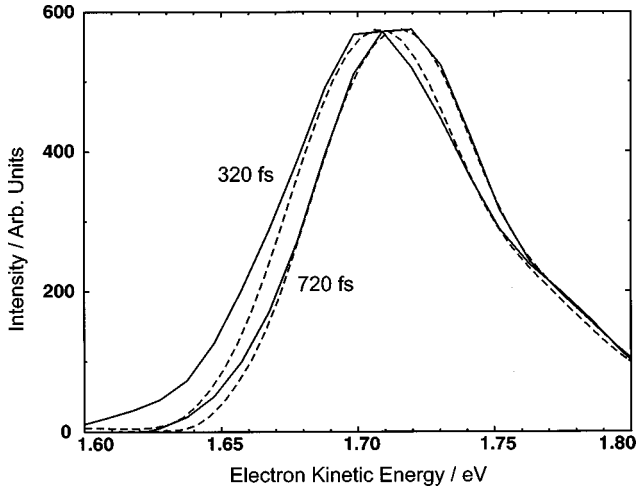

FIG. 3. Expanded view of the atomic $I(^2P_{3/2})\leftarrow I^-(^1S)$ feature at 1.71 eV. The experimental spectra (solid) shifts ~10 meV to higher energies from 320 to 720 fs. The simulated spectra (dashed) closely follows this trend.

background spectrum are due to transitions to the $\tilde{A}\,^3\Pi_{1u}$, $\tilde{A}'\,^3\Pi_{2u}$, and $\tilde{X}\,^1\Sigma_g^+$ states of neutral I_2, respectively.[25] This spectrum has been suitably scaled and subtracted from each of the two-photon spectra to remove the effects of ground state depletion by the pump pulse. Hence, these spectra reflect only the dynamics induced by the pump pulse.

The spectra in Fig. 2 are qualitatively similar to lower energy resolution spectra reported previously. In Fig. 2, one observes two broad features shifting toward lower energy as the delay time increases and evolving by 320 fs into two narrow peaks centered at 0.76 and 1.70 eV. Previously, the two narrow features were assigned to transitions from the I^- photoproduct to the $^2P_{1/2}$ and $^2P_{3/2}$ states of iodine, respectively, and the broad transients at earlier times were assigned to detachment of the dissociating wave packet on the $I_2^-(\tilde{A}'\,^2\Pi_{g,1/2})$ potential energy curve.

However, while the atomic features reach their maximum height by 320 fs, they undergo a 10 meV shift to higher kinetic energies over the next 400 fs, which actually brings them into better agreement with the atomic transitions for free I^- (which appear at 0.77 and 1.71 eV). This shift is shown in Fig. 3, where higher energy atomic features are expanded and compared at 320 fs and 720 fs. The energy shift is continuous and smooth over this time interval, and was not observed before in our earlier study on I_2^-, most likely due to our poorer electron energy resolution. As will be discussed below, the shift arises from the excited state wave packet traversing the long-range attractive portion of the I_2^- potential.

Since 1.71 eV corresponds to photodetachment of I^- products, a cut through the FPES spectra at this energy provides a measure of I^- production as a function of time. This is shown in Fig. 4 (solid). The half-maximum height is reached by 180 fs, and the full height at 320 fs. Repeated measurements of the experiment give a risetime which is reproduceable to within ±10 fs, and is considered our experimental error. The half-maximum height observed here is approximately 50 fs longer than our previously reported results.[29] This is again a result of our improved energy resolution which enables us to separate better the atomic and transient contributions to the spectra.

IV. ANALYSIS AND DISCUSSION

In this section we develop an $I_2^-(\tilde{A}'\,^2\Pi_{g,1/2})$ excited state potential that is accurate to within our experimental error by simulating the FPES spectra above 1.6 eV. To this end, we first explain the analytical potential used in the simulations, and our method of convoluting the simulated spectra. The simulations are then compared to experiment, error bars on the potential are estimated, and a comparison is made to previously reported potentials. Finally, the complete FPES

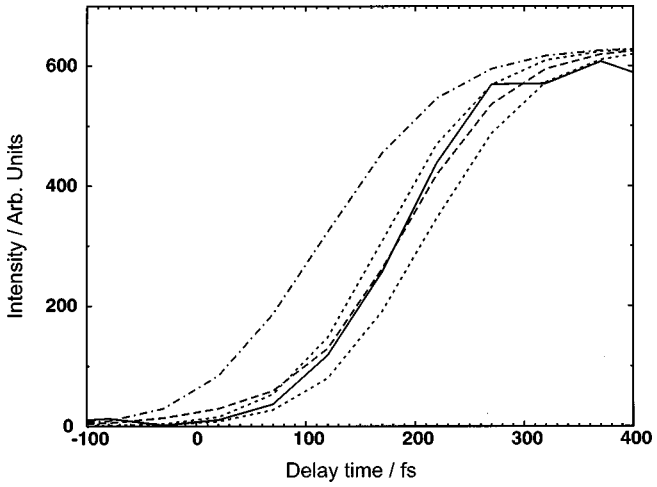

FIG. 4. Intensity at 1.71 eV plotted as a function of delay time, monitoring the appearance of I^- products. The experimental intensity (solid) reaches its half-maximum height by 180 fs and its full height by 320 fs. Risetimes for the best-fit potential (dashed), error-limit potentials (dotted), and the Chen and Wentworth potential (Ref. 26) (dotted–dashed) are also shown.

spectra are simulated using all 20 neutral potentials, and the accuracy of current I_2 *ab initio* potentials is commented on.

A. Analytical form of the $I_2^-(\tilde{A}'\,^2\Pi_{g,1/2})$ state

The FPES spectra are sensitive to three parts of the potential, listed in order of increasing internuclear distance: (1) the FC region, where the potential is repulsive, (2) the region in the vicinity of the attractive well, the existence of which is supported by the results in Fig. 3, and (3) the long-range attractive region. To effectively simulate the FPES spectra, a potential is needed which can be easily modified in these three areas. We have chosen Morse potentials to represent the first two regions, while the long-range attractive region is represented by a function which includes the charge-induced dipole (r^{-4}) and charge-induced quadrupole and dispersion (r^{-6}) terms. Two switching functions are used for transitions between regions. The analytical form for the entire potential is given in Eqs. (1) and (2),

$$\begin{aligned} V(r) &= 2D_e^1 \exp[-\beta^1(r-r_e^1)] + D_e^1 \exp[-2\beta^1(r-r_e^1)] \\ &\equiv v_1(r), \quad 0<r\leqslant r_1 \\ &= sf_1(r)v_1(r) + [1-sf_1(r)]v_2(r), \quad r_1<r\leqslant r_2 \\ &= 2D_e^2 \exp[-\beta^2(r-r_e^2)] + D_e^2 \exp[-2\beta^2(r \\ &\quad -r_e^2)] \equiv v_2(r), \quad r_2<r\leqslant r_3 \\ &= sf_2(r)v_2(r) + [1-sf_2(r)]v_3(r), \quad r_3<r\leqslant r_4 \\ &= -B_4/(D_e^2 r^4) - B_6/(D_e^2 r^6) \equiv v_3(r), \quad r_4<r<\infty, \end{aligned} \tag{1}$$

where

$$sf_n(r) = \frac{1}{2}\left(\cos\frac{\pi(r-r_n)}{r_{n+1}-r_n}+1\right). \tag{2}$$

$sf_n(r)$ are the switching functions connecting the three functions $v_n(r)$. D_e^n, r_e^n, and β^n are the well depth, equilibrium bond length, and beta parameter for each of the two Morse potentials. B_4 and B_6 are the charge-induced dipole and charge-induced quadrupole and dispersion terms, respectively, approximated with the parameters for XeI^-.[51] The parameters r_n in the two switching functions are chosen so that $v_1(r)$, $v_2(r)$, and $v_3(r)$ describe the three regions of the potential defined above.

The FC region is centered around $R=3.205$ Å, i.e., R_e for the I_2^- $\tilde{X}\,^2\Sigma_u^+$ state.[25] The potential in this region, along with the ground state wave function and photon energy, determines the initial wave function created on the excited state potential. To fit the potential in the FC region, we have simulated the photodissociation cross-section measurement carried out by Papanikolas *et al.*[15] on gas phase I_2^-. Their results are shown by the solid line in Fig. 5. Using a wave packet propagation code described earlier,[52] and assuming a temperature of 100 K for the I_2^-,[25] the cross section was simulated. Only the three parameters which determine $v_1(r)$ were adjusted to reproduce the maximum and width of the cross section, and the results are presented in Fig. 5 (dashed). This produces a reliable excited state potential in the FC region. In the simulations presented throughout the rest of this report, these three parameters are held fixed and only the remaining parameters are varied to fit the FPES spectra.

B. Convolution routine

Because we have found that the risetime of the $I(^2P_{3/2})$ spectra at 1.71 eV (Fig. 4) is very sensitive to the resolution of our spectrometer,[29] it is important to perform accurate convolutions of the simulated spectrum with the experimental resolution function. Previously an analytical form for the convolution function was used which had been derived based on the expected energy resolution of the magnetic bottle analyzer and the angular distribution of ejected electrons.[29] Here an improved procedure is employed, in which the simulations are convoluted with an empirical resolution function derived from the photoelectron spectrum of I^-.

The standard convolution formula is used,

$$g_{\text{conv}}(\epsilon) = \int_{-\infty}^{\infty} f(E)\cdot g(\epsilon - E)\,dE, \tag{3}$$

where $g(\epsilon)$ is the simulated spectrum and $f(E)$ is the convolution function. In our routine, $f(E)$ assumes the experimental I^- features at their respective electron energies of 0.12, 0.77, and 1.71 eV; the first peak is obtained at a detachment wavelength of 390 nm, and the second two at 260 nm. At other electron energies, the convolution function is computed by interpolation (or extrapolation) of the two nearest experimental I^- features. This guarantees that at long times, when the experimental spectrum only consists of atomic features, the simulated and experimental spectra will match. It also helps ensure that the risetime of the I^- feature at 1.71 eV is accurately modeled with the current experimental resolution. However, the procedure implicitly assumes that at all time delays the angular distribution is the same as for I^- photodetachment. The effect of the angular distribution on the photoelectron spectra diminishes when the ion

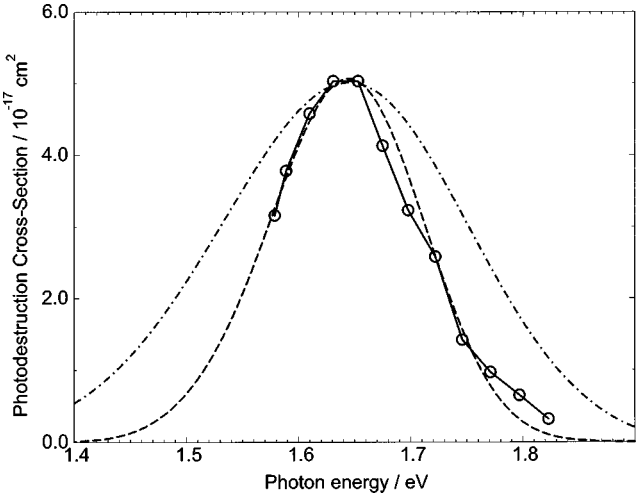

FIG. 5. Photodestruction cross-section measurement (Ref. 15) (solid circles) and simulations using the best-fit potential (dashed) and the Chen and Wentworth potential (Ref. 26) (dotted–dashed).

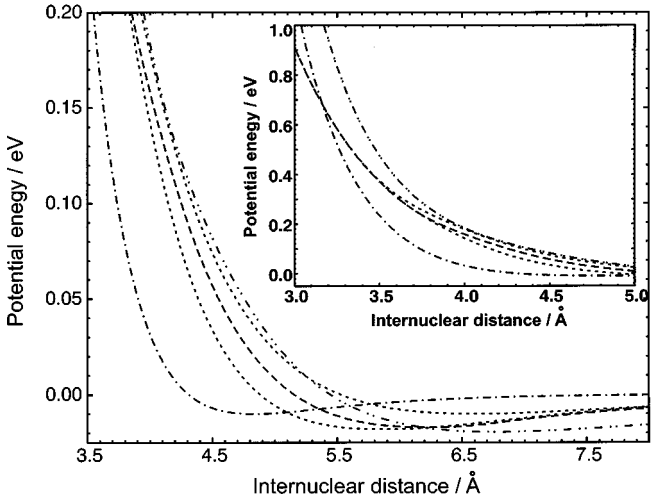

FIG. 6. Comparison of our potential (dashed) with estimated error limits (dotted) to the Chen and Wentworth potential (Ref. 26) (dotted–dashed), and *ab initio* potential (Refs. 40–42) (double dotted–dashed). Inset shows the FC region of the potentials.

beam is slowed down, as was the case here,[29,47] and plays a much smaller role in this report than in our original study.

C. Simulated FPES spectra above 1.7 eV

With the first three parameters fixed to reproduce the photodestruction cross section, the other ten parameters were varied and the FPES spectra simulated. In our companion paper,[44] we discuss the exact method for simulating the spectra. In this paper, we concentrate only on the results of these simulations. In addition, for the purpose of determining an accurate $I_2^-(\tilde{A}'\,^2\Pi_{g,1/2})$ excited state potential, only the spectrum from 1.6 eV and above was modeled (Fig. 2, solid). This region of the spectrum corresponds to detachment to the neutral potentials which correlate to $I(^2P_{3/2})+I(^2P_{3/2})$ products. These potentials are considerably better characterized than the potentials correlating to $I(^2P_{3/2})+I^*(^2P_{1/2})$ products.

Simulations from the optimized $I_2^-(\tilde{A}'\,^2\Pi_{g,1/2})$ potential are shown in Fig. 2 (dashed), superimposed on the experimental spectrum. The potential itself is shown in Fig. 6 (dashed), and its parameters are given in Table I. For the purpose of determining the $I_2^-(\tilde{A}'\,^2\Pi_{g,1/2})$ excited state, the simulations include photodetachment to the lowest 10 states of neutral I_2 which correlate to $I(^2P_{3/2})+I(^2P_{3/2})$ products, seven of which have been characterized experimentally; the $\tilde{X}\,^1\Sigma_g^+$, $\tilde{A}'\,^3\Pi_{2u}$, $\tilde{A}\,^3\Pi_{1u}$, $\tilde{B}'\,^3\Pi_{0_u^-}$, $\tilde{B}''\,^1\Pi_u$, $\tilde{a}\,^3\Pi_{1g}$, and the $\tilde{a}'\,^3\Sigma^-_{g(0^+)}$ states.[30–36] From *ab initio* work,[53,54] the $^3\Pi_{2g}$ and $\tilde{a}\,^3\Pi_{1g}$ states are predicted to be nearly degenerate, as are the $^3\Sigma^-_{u(0^-)}$ and $^3\Delta_{3u}$ states with the $\tilde{a}'\,^3\Sigma^-_{g(10^+)}$ state. Hence, we approximate these three experimentally undetermined states by their degenerate counterparts.

TABLE I. Spectroscopic constants for the $I_2^-(\tilde{A}'\,^2\Pi_{g,1/2})$ potential in Eqs. (1) and (2).

$v_1(r)$	$r_e^1=0.01$ Å	$sf_1(r)$	$r_1=3.4$ Å
	$D_e^1=6.000$ eV		$r_2=4.2$ Å
	$\beta^1=0.787$ Å^{-1}		
$v_2(r)$	$r_e^2=0.017$ Å	$sf_2(r)$	$r_3=8.4$ Å
	$D_e^2=6.20$ eV		$r_4=9.0$ Å
	$\beta^2=0.663$ Å^{-1}		
$v_3(r)$	$B_4=28.977$ eV Å[a]		
	$B_6=365.448$ eV Å[a]		

[a]Reference 51.

Several of these neutral states are not accessible by one-electron detachment from the $I_2^-(\tilde{A}'\,^2\Pi_{g,1/2})$ excited state. However, as discussed by Faeder and Parson,[43] the large spin–orbit coupling of iodine mixes the electronic configurations to such an extent that only transitions to the $I_2\ \tilde{X}\,^1\Sigma_g^+$ state are predicted to be forbidden. Thus, equal weightings are assumed for transitions to all neutral states except the $\tilde{X}\,^1\Sigma_g^+$ state, for which the detachment cross section is set to zero.

Comparison of the simulated and experimental data in Fig. 2 (dashed) shows excellent agreement. The high energy features from 1.8 to 2.3 eV match the experiment well, and the rise of the I^- feature at 1.70 eV is followed closely. The intensity at 1.75 eV is slightly underrepresented at delay times of 170, 220, and 270 fs. Comparison of the simulated risetime to experiment shows that the half-maximum height is reproduced at 180 fs, although the slope is not as steep (Fig. 4, dashed). This may be due to the simulated pulsewidths being slightly too long in duration. Finally, a comparison of the energy shift observed between 420–700 fs is shown in Fig. 3 (dashed). At 420 fs the simulated spectra is approximately 2 meV higher in energy than experiment, and smoothly shifts to 1.71 eV over the next 300 fs.

These results represent a significant improvement over our previous study of I_2^- photodissociation.[29] As has been found by Faeder and Parson,[43] inclusion of the additional neutral potentials helps improve the fit to the transient intensities. We find that this does indeed improve the agreement, especially at energies above 1.8 eV, although modification of the $I_2^-(\tilde{A}'\,^2\Pi_{g,1/2})$ potential itself was the largest factor in improving the fits.

Several assumptions are implicit in our calculations. First, the oscillator strengths for transitions from the $I_2^-(\tilde{A}'\,^2\Pi_{g,1/2})$ anion to the neutral states are unknown. From the study of Asmis *et al.*,[55] it was found that detachment from the *ground* $\tilde{X}\,^2\Sigma_u^+$ state of I_2^- to the $\tilde{B}'\,^3\Pi_{0_u^-}$ and $\tilde{B}''\,^1\Pi_u$ states of I_2 is only $\frac{1}{3}$ as intense as detachment to the $\tilde{A}'\,^3\Pi_{2u}$ and $\tilde{A}\,^3\Pi_{1u}$ states. When using their weights for photodetachment from the $I_2^-(\tilde{A}'\,^2\Pi_{g,1/2})$ state, however, the transient intensities are not as well represented as when all oscillator strengths are assumed to be the same. In fact, for a proper fit of the photoelectron spectra, transitions to the $\tilde{a}\,^3\Pi_{1g}$ and $^3\Pi_{2g}$ states must be included, even though these states are normally forbidden, lending support to the conclusion of Faeder and Parson[55] that the one-electron transition rule is relaxed by the strong spin–orbit coupling. We have also individually varied the relative weightings of all the states, and found that the risetime (Fig. 4) is insensitive to

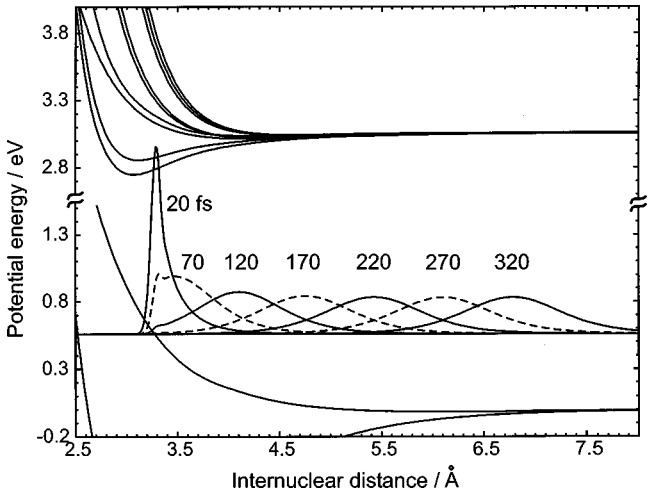

FIG. 7. Simulated wave functions corresponding to the experimental spectra delay times. The wave function does not fully reach the bottom of the $I_2^-(\tilde{A}'\,^2\Pi_{g,1/2})$ well until 270 fs.

the individual weights. In fact, except for the $\tilde{a}'\,^3\Sigma^-_{g(0^+)}$ state, the individual risetimes of all the neutral states lie within ± 10 fs of one another. Thus, the risetime is almost solely determined by the anion potential, at least for reasonably well characterized neutral states.

The second important assumption is that the photodetachment transition dipole moments are independent of nuclear coordinates. This is certainly not correct, although we have no means for calculating these moments. However, this approximation should only affect the relative intensity between the transient features above 1.8 eV and the I^- feature at 1.71 eV; the risetime should again remain unaffected.

Further insight into the photoelectron spectra can be gained by examining the time-dependence of the excited state anion wave function, which is also calculated as part of the quantum mechanical propagation method.[44] Shown in Fig. 7 are the wave functions at the experimental delay times superimposed on the anion and neutral potential energy surfaces. At 20 fs pump–probe delay, the wave packet mostly resides in the FC region. At this time delay, detachment of the wave packet produces a broad spectrum because of the large splittings between the neutral potential energy curves. The spectrum is also centered at higher electron energies than at longer times because the vertical detachment energies are lower, on the average. At 170 fs, the breadth of the spectra is almost entirely due to the slope of the anion potential since the neutral potentials have nearly reached their asymptotic values. The transient intensity in the simulated spectra does not disappear, however, until about 270 fs at which point the wave packet resides in the region of the shallow anion potential well. At this internuclear distance the neutral potentials are all within 4 meV of their asymptotic energies. The anion potential, however, is 17 meV lower than its asymptotic energy. Thus, the shift to higher energies over the next 400 fs is due to the wave packet moving out of the anion potential well. By 700 fs, the experimental spectrum no longer shifts with time, and the effect of attractive interactions on the anion potential has become insignificant.

TABLE II. Comparison of D_e and R_e with previously reported potentials.

	Current work	*ab initio*[a]	Chen and Wentworth[b]	Dojahn *et al.*[c]	Chen *et al.*[d]
R_e (Å)	6.2 ± 0.6	6.8	4.83	4.626	4.70
D_e (eV)	0.017 ± 0.010	0.0195	0.01	0.08	0.057[e]

[a]References 40–42.
[b]Reference 26.
[c]Reference 27.
[d]Reference 28.
[e]Reported value is $D_0 = 0.056$ eV. D_e determined by adding 0.001 eV zero point energy.

From the simulations, this corresponds to an internuclear distance of about 11 Å.

In order to estimate the error in our potential, the FPES spectra were simulated for two additional potential surfaces with slightly more repulsive and attractive potentials. These potentials are shown in Fig. 6 (dotted), along with the best-fit potential described above (dashed). All three potentials are identical in the FC region of the potential (Fig. 6, inset). The simulated FPES spectra are not shown, but the risetimes at 1.71 eV are compared in Fig. 4 (dotted) to the best-fit (dashed) and experimental risetimes (solid). The potential with the steeper slope for $R < R_e$ produces a faster risetime because the wave packet reaches the asymptotic region more rapidly. Conversely, the potential with the shallower slope results in slower dissociation and a slower risetime. Although these two potentials do not fit the experimental risetimes as well, they are not necessarily bad fits. We believe they represent reasonable error limits in our determination of the $I_2^-(\tilde{A}'\,^2\Pi_{g,1/2})$ state, and are used to estimate error bars for the parameters listed in Table II.

D. Comparison with previous potentials

Table II compares our well depth and equilibrium bond length to the three semiempirical potentials proposed by Chen and Wentworth,[26–28] and the *ab initio* potential by Maslen *et al.*[40] As was the case in our previous determination of the $I_2^-(\tilde{X}\,^2\Sigma_u^+)$ ground state potential,[25] the original $I_2^-(\tilde{A}'\,^2\Pi_{g,1/2})$ semiempirical potential published[26] in 1985 matches our parameters more closely than the later two potentials.[27,28] As is seen in Fig. 6 (dotted–dashed), however, even the original potential lies well outside our limits of error. It has a comparable well depth, but the well itself is located at much smaller internuclear distances, which produces a repulsive wall that is considerably steeper than predicted by our simulations.

As an indication of the sensitivity of our spectra to the shape of the excited state potential, we have simulated the spectra using our $I_2^-(\tilde{X}\,^2\Sigma_u^+)$ ground state and Chen and Wentworth's $I_2^-(\tilde{A}'\,^2\Pi_{g,1/2})$ excited state potential from 1985.[26] Figure 8 compares the simulations (dashed) to experiment (solid). Note that the transient intensity above 1.8 eV is almost completely missing, even at 20 fs delay time, and the atomic feature forms much too early. Indeed, the simulated risetime occurs 70 fs faster than the experiment (Fig. 4, dotted–dashed), and the atomic feature rises directly

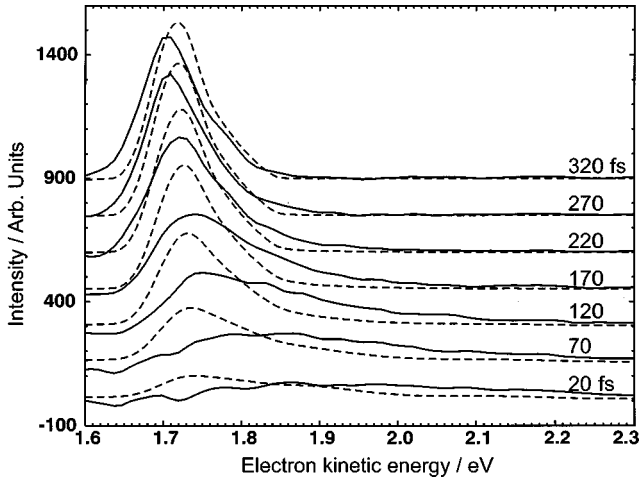

FIG. 8. Comparison of the experimental spectra (solid) to simulations (dashed) using the Chen and Wentworth potential (Ref. 26).

at 1.71 eV with no energy shift. These discrepancies indicate that this potential is too repulsive at short internuclear distances and not attractive enough at long internuclear distances, both consequences of R_e being too small. We have also calculated the photodestruction cross section using this potential and find it to be much too wide (Fig. 5, dotted–dashed), showing that the potential is too steep in the FC region. It seems unlikely that a single Morse potential for the $I_2^-(\tilde{A}'\,^2\Pi_{g,1/2})$ state will suffice to fit all the experimental data now available.

The well depth and internuclear distance for the *ab initio* potential[40–42] are in remarkably good agreement with our results (Fig. 6, double dotted–dashed). Its well depth $D_e = 19.5\,\text{meV}$ and equilibrium internuclear distance $R_e = 6.8\,\text{Å}$ lie within our estimated error bars. At smaller internuclear distances, however, the *ab initio* potential diverges from ours, and is ~300 meV too high in energy at the FC region (Fig. 6, inset). This seems to indicate that the *ab initio* methods are reliable in predicting long-range electrostatic interactions, and may be expected to accurately represent the excited state wells of other diatomic anions.

E. Simulation of the entire FPES spectrum

With the determination of a reliable $I_2^-(\tilde{A}'\,^2\Pi_{g,1/2})$ state, the entire FPES spectra can now be simulated by including the remaining 10 neutral states correlating to $I(^2P_{3/2}) + I^*(^2P_{1/2})$ products. Very little is known about these states; only the $\tilde{B}\,^3\Pi_{0^-u}$ has been spectroscopically determined.[32] Information on the other states comes from relativistic *ab initio* calculations by Li *et al.*,[56] Teichteil *et al.*,[53] and de Jong *et al.*[54] By simulating the region of the FPES spectra corresponding to these states (i.e. at electron energies below 1.6 eV) and comparing with experiment, the accuracy of the *ab initio* potentials can be evaluated.

Following the procedure described above, the entire photoelectron spectrum was simulated using the potentials calculated by de Jong *et al.*[54] (Fig. 2, dotted) and those used above (Fig. 2, dashed). Transitions to all states in the $I(^2P_{3/2}) + I^*(^2P_{1/2})$ manifold have been equally weighted, although their integrated intensity has been reduced by a factor of ~2 to reproduce the intensity of the $I(^2P_{1/2}) \leftarrow I^-$ transition at 0.77 eV. The agreement is far from perfect, however, for the formation of the $I^*(^2P_{1/2})$ peak. Except for the contribution of the $\tilde{B}\,^3\Pi_{0^-u}$ state (which extends up to 1.5 eV, but at intensities too low to observe in Fig. 2), the simulations produce transient features from 0.6 to 0.9 eV, with no dominant features. The experiment, however, has intensity up to 1.0 eV, which indicates that the neutral states are at least 100 meV too high in energy at the FC region. In addition, sharp features at 0.85 and 0.95 eV are seen in the experiment at −30 fs; although similar in appearance to the background peaks labeled A and B in Fig. 2, these features are true transients and not artifacts of background subtraction. Each sharp feature arises from detachment to one or more neutral states, largely separated from adjacent states. The absence of these features in the simulations indicates that the *ab initio* potential energy curves are too evenly spaced in the FC region. Finally, the rise of the $I^*(^2P_{1/2})$ feature is much faster than experiment, and the transient intensity is too small, both suggesting that the I_2 states are ''too parallel'' to the $I_2^-(\tilde{A}'\,^2\Pi_{g,1/2})$ state.

V. CONCLUSION

The feasibility of using femtosecond photoelectron spectroscopy to determine excited anion state potentials is demonstrated. The first quantitative excited state potential for the $I_2^-(\tilde{A}'\,^2\Pi_{g,1/2})$ excited state of I_2^- is reported, which has been fit to a piecewise potential by simulation of the spectra. Careful consideration has been given to the accuracy of our fit, and reasonable error limits have been assigned. We find the potential contains a shallow well located at large internuclear distances, in qualitative agreement with a recent *ab initio* calculation but not with previously proposed semiempirical potentials. Comparison of the spectra to calculated wave functions reveals FPES to be sensitive to the repulsive wall, the potential well, and the long-range attractive portions of the potential. The accuracy of current *ab initio* potentials for the $I(^2P_{3/2}) + I^*(^2P_{1/2})$ manifold is also assessed. The extension of this type of analysis to higher dimensional systems, and to systems with a larger excited state wells are being investigated.

ACKNOWLEDGMENTS

D.M.N. acknowledges support from the National Science Foundation under Grant No. CHE-9710243 and from the Defense University Research Instrumentation Program under Grant No. F49620-95-0078. W.H.M. acknowledges support from the National Science Foundation under Grant No. CHE-9732758, from the Director, Office of Energy Research, Office of Basic Energy Sciences, Chemical Sciences Division of the U.S. Department of Energy under Contract No. DE-AC03-76SF00098, and from the Laboratory Directed Research and Development (LDRD) project from the National Energy Research Scientific Computing Center (NERSC), Lawrence Berkeley National Laboratory. The au-

thors also thank Jim Faeder for helpful suggestions and Robert J. LeRoy for providing the RKRI algorithm for use in calculating the I_2 states.

[1] Q. L. Liu, J. K. Wang, and A. H. Zewail, Nature (London) **364**, 427 (1993).
[2] J. K. Wang, Q. L. Liu, and A. H. Zewail, J. Phys. Chem. **99**, 11309 (1995).
[3] T. J. Chung, G. W. Hoffman, and K. B. Eisenthal, Chem. Phys. Lett. **25**, 201 (1974).
[4] P. Bado, C. Dupuy, D. Magde, K. R. Wilson, and M. M. Malley, J. Chem. Phys. **80**, 5531 (1984).
[5] P. Bado and K. R. Wilson, J. Phys. Chem. **88**, 655 (1984).
[6] D. F. Kelly, N. A. Abul-Haj, and D. J. Jang, J. Chem. Phys. **80**, 4105 (1984).
[7] D. E. Smith and C. B. Harris, J. Chem. Phys. **87**, 2709 (1987).
[8] A. L. Harris, J. K. Brown, and C. B. Harris, Annu. Rev. Phys. Chem. **39**, 341 (1988).
[9] N. F. Scherer, L. D. Ziegler, and G. R. Fleming, J. Chem. Phys. **96**, 5544 (1992).
[10] N. F. Scherer, D. M. Jonas, and G. R. Fleming, J. Chem. Phys. **99**, 153 (1993).
[11] R. Zadoyan, Z. Li, P. Ashjian, C. C. Martens, and V. A. Apkarian, Chem. Phys. Lett. **218**, 504 (1994).
[12] R. Zadoyan, Z. Li, C. C. Martens, and V. A. Apkarian, J. Chem. Phys. **101**, 6648 (1994).
[13] V. Vorsa, S. Nandi, P. J. Campagnola, M. Larsson, and W. C. Lineberger, J. Chem. Phys. **106**, 1402 (1997).
[14] B. J. Greenblatt, M. T. Zanni, and D. M. Neumark, Science **276**, 1675 (1997).
[15] J. M. Papanikolas, J. R. Gord, N. E. Levinger, D. Ray, V. Vorsa, and W. C. Lineberger, J. Phys. Chem. **95**, 8028 (1991).
[16] J. M. Papanikolas, V. Vorsa, M. E. Nadal, P. J. Campagnola, H. K. Buchenau, and W. C. Lineberger, J. Chem. Phys. **99**, 8733 (1993).
[17] B. J. Greenblatt, M. T. Zanni, and D. M. Neumark, Faraday Discuss. **108**, 101 (1998).
[18] A. Sanov, S. Nandi, and W. C. Lineberger, J. Chem. Phys. **108**, 5155 (1998).
[19] A. E. Johnson, N. E. Levinger, and P. F. Barbara, J. Phys. Chem. **96**, 7841 (1992).
[20] I. Benjamin, P. F. Barbara, B. J. Gertner, and J. T. Hynes, J. Phys. Chem. **99**, 7557 (1995).
[21] P. K. Walhout, J. C. Alfano, K. A. M. Thakur, and P. F. Barbara, J. Phys. Chem. **99**, 7568 (1995).
[22] U. Banin and S. Ruhman, J. Chem. Phys. **99**, 9318 (1993).
[23] U. Banin and S. Ruhman, J. Chem. Phys. **98**, 4391 (1993).
[24] T. Kuhne and P. Vohringer, J. Chem. Phys. **105**, 10788 (1996).
[25] M. T. Zanni, T. R. Taylor, B. J. Greenblatt, B. Soep, and D. M. Neumark, J. Chem. Phys. **107**, 7613 (1997).
[26] E. C. M. Chen and W. E. Wentworth, J. Phys. Chem. **89**, 4099 (1985).
[27] J. G. Dojahn, E. C. M. Chen, and W. E. Wentworth, J. Phys. Chem. **100**, 9649 (1996).
[28] E. C. M. Chen, J. G. Dojahn, and W. E. Wentworth, J. Phys. Chem. A **101**, 3088 (1997).
[29] B. J. Greenblatt, M. T. Zanni, and D. M. Neumark, Chem. Phys. Lett. **258**, 523 (1996).
[30] S. Churassy, F. Martin, R. Bacis, J. Verges, and R. W. Field, J. Chem. Phys. **75**, 4863 (1981).
[31] K. S. Viswanathan and J. Tellinghuisen, J. Mol. Spectrosc. **101**, 285 (1983).
[32] J. W. Tromp and R. J. Le Roy, J. Mol. Spectrosc. **109**, 352 (1985).
[33] J. Tellinghuisen, J. Chem. Phys. **82**, 4012 (1985).
[34] F. Martin, R. Bacis, S. Churassy, and J. Verges, J. Mol. Spectrosc. **116**, 71 (1986).
[35] X. N. Zheng, S. L. Fei, M. C. Heaven, and J. Tellinghuisen, J. Chem. Phys. **96**, 4877 (1992).
[36] D. R. T. Appadoo, R. J. Leroy, P. F. Bernath, S. Gerstenkorn, P. Luc, J. Verges, J. Sinzelle, J. Chevillard, and Y. Daignaux, J. Chem. Phys. **104**, 903 (1996).
[37] P. W. Tasker, G. G. Balint-Kurti, and R. N. Dixon, Mol. Phys. **32**, 1651 (1976).
[38] G. A. Bowmaker, P. Schwerdfeger, and L. v. Szentpaly, J. Mol. Struct.: THEOCHEM **53**, 87 (1989).
[39] D. Danovich, J. Hrusak, and S. Shaik, Chem. Phys. Lett. **233**, 249 (1995).
[40] P. E. Maslen, J. Faeder, and R. Parson, Chem. Phys. Lett. **263**, 63 (1996).
[41] J. Faeder, N. Delaney, P. E. Maslen, and R. Parson, Chem. Phys. Lett. **270**, 196 (1997).
[42] J. Faeder, N. Delaney, P. E. Maslen, and R. Parson, Chem. Phys. **239**, 525 (1999).
[43] J. Faeder and R. Parson, J. Chem. Phys. **108**, 3909 (1998).
[44] V. S. Batista, M. T. Zanni, B. J. Greenblatt, D. M. Neumark, and W. H. Miller, J. Chem. Phys. **110**, 3736 (1998), preceding paper.
[45] R. Prosch and T. Trickl, Rev. Sci. Instrum. **60**, 713 (1989).
[46] W. C. Wiley and I. H. McLaren, Rev. Sci. Instrum. **26**, 1150 (1955).
[47] O. Cheshnovsky, S. H. Yang, C. L. Pettiette, M. J. Craycraft, and R. E. Smalley, Rev. Sci. Instrum. **58**, 2131 (1987).
[48] H. Handschuh, G. Gantefor, and W. Eberhardt, Rev. Sci. Instrum. **66**, 3838 (1995).
[49] L.-S. Wang, H.-S. Cheng, and J. Fan, J. Chem. Phys. **102**, 9480 (1995).
[50] M. D. Davidson, B. Broers, H. G. Muller, and H. B. v. L. v. d. Heuvell, J. Phys. B **25**, 3093 (1992).
[51] T. Lenzer, M. R. Furlanetto, K. R. Asmis, and D. M. Neumark, J. Chem. Phys. **109**, 10754 (1998).
[52] S. E. Bradforth, A. Weaver, D. W. Arnold, R. B. Metz, and D. M. Neumark, J. Chem. Phys. **92**, 7205 (1990).
[53] C. Teichteil and M. Pelissier, Chem. Phys. **180**, 1 (1994).
[54] W. A. de Jong, L. Visscher, and W. C. Nieuwpoort, J. Chem. Phys. **107**, 9046 (1997).
[55] K. R. Asmis, T. R. Taylor, C. Xu, and D. M. Neumark, J. Chem. Phys. **109**, 4389 (1998).
[56] Q. Li and K. Balasubramanian, J. Mol. Spectrosc. **138**, 162 (1989).